Hindawi
Geofluids
Volume 2024, Article ID 5525827, 10 pages
https://doi.org/10.1155/2024/5525827

Research Article

Development and Application of a Percolation Velocity Monitoring Method in Multiphase Percolation Physical Experiments

Cuo Guan,[1,2] **Xianjie Li**,[1,2] **Ke Hu**,[1,2] **Chen Liu**,[1,2] **Hong Du**,[1,2] **and Ruokun Xian**[1,2]

[1]*State Key Laboratory for Efficient Development of Offshore Oil, Beijing, China*
[2]*CNOOC Research Institute Co., Ltd., Beijing, China*

Correspondence should be addressed to Cuo Guan; guancuo@163.com

Received 18 August 2023; Revised 4 February 2024; Accepted 22 February 2024; Published 20 April 2024

Academic Editor: Qingchao Li

Unlike conventional single-phase seepage monitoring methods, monitoring multiphase flow in porous media is more complex. This paper addresses this complexity by analyzing the heat transfer in porous media models under multiphase seepage conditions. It introduces a set of theories, methods, and devices to effectively monitor the flow velocity in multiphase seepage processes. Utilizing a self-developed single-point self-heating temperature-sensing device combined with saturation testing at monitoring points, we establish a method to determine the relationship between different saturation and resistivity, as well as the saturation and thermal conductivity of the reservoir model, which provides essential parameter support for the calculation of results during flow velocity monitoring. The effectiveness of the flow velocity monitoring method was confirmed through a one-dimensional constant velocity multiphase seepage experiment. Furthermore, oil-water two-phase seepage simulation experiments were conducted based on the sandpack model. By comparing the real oil-water flow velocity with the monitored velocity, the accuracy can reach over 95%, validating the accuracy and reliability of the method proposed in this paper. The seepage flow velocity monitoring theory and technology established herein offer corresponding theories and methods for obtaining fluid seepage velocity in porous media with multiphase fluids.

1. Introduction

Seepage monitoring not only involves determining whether leakage occurs but also includes the accurate positioning of the leakage location, the path of leakage occurrence, and the precise reflection of the leakage rate (as shown in Figure 1). Currently, it is mainly applied in pipeline transportation, reservoir dams, and river channel earth-rockfill dam leakage monitoring [1–3].

At present, there are many effective methods to detect the fluid seepage condition in porous media. The high-density electrical method is a geological tomography technology that integrates electrical profiling and electrical sounding methods. The host provides power to the earth through a pair of power supply electrodes and employs a pair of observation electrodes to measure electrical parameters, such as potential and current, point by point along the profile. The high-density electrical method instrument automatically records and calculates the apparent resistivity values of each measurement point. The spatial distribution characteristics of the underground electrical layer in the profile are determined through computer analysis and processing of the apparent resistivity profile. Comprehensive analysis of apparent resistivity profile anomalies are comprehensively analyzed in conjunction with relevant data, allowing speculation regarding the presence of water seepage areas, structural fracture zones, etc., within the strata of the survey line location.

The transient electromagnetic method is based on the principle of electromagnetic induction, which relies on the electrical (magnetic) differences of the medium. It emits a vertical primary pulse magnetic field into the ground through an ungrounded return line or a grounded electrode, triggering the low-resistance medium within the ground to

Leakage monitoring of oil and water transportation pipelines

Dam leakage monitoring

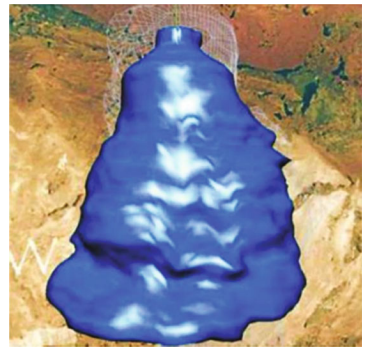

Leakage detection of gas storage sealing

Figure 1: Some application fields of percolation monitoring.

produce induced eddy currents, which subsequently generate a secondary magnetic field. By observing and studying the spatial and temporal distribution characteristics of this secondary field, we can explore the properties and distribution characteristics of the underground medium. Electromagnetic detection possesses a high level of sensitivity, directness, and intuition for leakage detection. However, there is a lack of research exploring the relationship between the physical properties of soil media, such as water content and the porosity of the dam body, and the electrical resistivity of the leakage medium. The discussion regarding the criteria for judging the leakage of rock and soil media is inadequate; thus, further research is required for quantitative evaluation.

The seismic imaging method is developed based on the optimal offset technology in seismic reflection waves. It employs either equal offset or zero offset to stimulate wideband elastic waves, swiftly and densely collect images of the elastic wave field, and document (record) direct waves, surface waves, diffraction waves, reflection waves, etc. By analyzing the features of diffraction waves, reflection waves, etc., in the records, the distribution of anomalous bodies underground can be quickly ascertained. It can approximate a complex two-dimensional or three-dimensional problem to a one-dimensional problem. Compared to the conventional multiple coverage reflection wave method, the wave field is simple and intuitive, requiring less processing, offering interpretation and real-time performance.

The fluorescent tracer method can offer a novel approach for the investigation of dam leaks. Currently, this method is predominantly employed in the research of groundwater within porous and karst aquifers. The method primarily encompasses injecting a specific concentration of tracer at designated locations, monitoring observation points, and subsequently determining the characteristics of the medium.

The theoretical basis of thermal monitoring technology for earth-rock dams relies on the coupling between the seepage field and temperature field (flow-heat) in the rock and soil mass. The migration of moisture within the medium governs the temperature field's distribution, while the spatial and temporal temperature distribution can inversely reflect the characteristics of the seepage field. The temperature difference measured before and after leakage occurs can be used to pinpoint the location of the leakage. Concentrated leakage will result in alterations of the temperature field distribution of the dam body. By analyzing the temperature field of the medium around the optical fiber, the location of leakage in the dam body can be determined.

In addition to the above detection methods, seepage detection also includes flow field methods, cross-well seismic CT technology, ultrasonic logging, and in-hole television detection methods (as shown in Table 1).

And good practical results can be achieved from both theoretical methods and on-site application conditions [12–14]. However, the above research and application mostly focus on the conditions of single-phase fluid flow, and currently, there is a lack of methods and theories for monitoring the two-phase flow velocity in porous media.

Multiphase seepage is widespread in fields such as oil and gas field development. Effective monitoring of the velocity of each phase in the multiphase seepage process in porous media can provide powerful parameter support for intuitively exploring (understanding) the laws of multiphase. During the indoor water flooding process, due to the difficulty of directly measuring flow velocity, currently, the two-phase flow velocity is calculated using the monitored oil saturation, pressure distribution, and other parameters, combined with Darcy's equation. When multiphase mixed flow is involved in a formation, unlike conventional single-phase flow monitoring methods, the monitoring of seepage flow becomes more complex due to the constantly changing fluid content in the reservoir [15–17].

To enhance the accuracy and efficiency of monitoring multiphase flow velocity during the indoor multiphase percolation experiment, a single-point self-heating temperature-sensing device combined with a corresponding saturation testing method is developed based on the analysis of heat transfer in porous media, which helps to effectively monitor the flow velocity during multiphase percolation.

2. Basic Assumptions for Heat Transfer Analysis in the Model

The fundamental theoretical foundation for monitoring seepage flow in porous media involves the self-heating

Table 1: Common detection methods of seepage velocity.

Method	Advantage	Limitations/disadvantages
Electrical detection [4–6]	Widely applicable conditions	The mechanism of action is unclear, and the resolution is low
Electromagnetic detection [7, 8]	Quick and intuitive	There are too many influencing factors to quantitatively describe
Elastic wave method [9, 10]	Intuitive monitoring methods	Not significantly effective for small-scale detection
Tracer method [11]	Ability to monitor the leakage channel and determine the leakage speed	Radioactivity and contamination of tracers
Temperature change [11]	High testing accuracy, which can reflect changes in flow velocity	The respective velocity of multiphase flow cannot be reflected

temperature-sensing device adding heat transfer and convection terms between the seepage flow location and the porous media (as shown in Figure 2). This leads to a temperature difference compared to nonseepage flow conditions. The fluid flow velocity in porous media is related to the heat loss of the self-heating temperature-sensing device. The temperature distribution map measured by the monitoring system is combined with theoretical analysis to achieve the judgment and calculation of the location and flow velocity of seepage flow.

The heat transfer modes between the self-heating temperature-sensing device and the reservoir model are complex, and it is impossible to consider all factors. Therefore, the following assumptions are made during this study:

(1) The heat exchange between the self-heating temperature-sensing device and the nearby reservoir model is considered as one-dimensional heat transfer

(2) The thermal radiation effect of the self-heating temperature-sensing device is not considered

(3) Since the water flooding experiments were conducted at a relatively low temperature (<100°C), there were no phase change and heat transfer during the entire process

(4) The reservoir model is completely saturated with oil and water, with no air present

Changes in ambient temperature can significantly impact the physical and chemical properties of the reservoir model and its internal fluids, which may lead to changes in the percolation characteristics of the reservoir model to some extent. For the reservoir model, fluctuations in temperature within the range of 10°C will not produce significant fluctuations in the values. Throughout the testing process, the temperature rise of the self-heating temperature-sensing device will be controlled within 10°C to simplify the calculation process and reduce the model's complexity, thereby neglecting the impact of temperature changes on the physical and chemical properties of the reservoir model. Concerning the fluid in the reservoir model, the corresponding parameters that affect the percolation law are density and specific gravity. Previous studies have indicated that a temperature change of 5-10°C will result in less than 0.2% fluctuations in the parameters of water density and specific gravity. The fluctuation in thermal conductivity and expansion coefficient is less than 2%, and the viscosity change rate is approximately 10%. This study is to explore the impact of the velocity field of the reservoir model on the temperature field and to quantify the percolation condition in the reservoir model using the self-heating sensing device. Therefore, the impact of temperature changes on percolation is not considered [18].

For self-heating temperature-sensing devices, when both internal heat conduction and surface heat transfer take place, if the latter value is significantly larger than the former, internal heat conduction occurs in a very small time; that is, the internal temperature distribution instantaneously balances. The Biot number (Bi) is an important dimensionless criterion number in thermal conductivity analysis, which characterizes the comparative relationship between the thermal resistance of heat conduction within the system and its surface convection heat transfer resistance.

For objects of arbitrary shape,

$$B_i = \frac{\delta h}{\lambda} < 0.1, \tag{1}$$

and also,

$$\frac{\theta}{\theta_m} = \frac{t_o - t_i}{t_{om} - t_{im}} > 0.95, \tag{2}$$

where λ is the thermal conductivity (W/(m·°C)); h is the convective heat transfer coefficient (W/(m·°C)); δ is the characteristic length, dimensionless; t_o is the excess temperature inside the heating device (°C); t_i is the initial temperature inside the heating device (°C); t_i is the final temperature inside the heating device (°C); θ_m is the excess temperature on the surface of the heating device (°C); t_{om} is the initial temperature on the surface of the heating device (°C); and t_{im} is the final temperature on the surface of the heating device (°C).

In a narrow temperature range, the ratio of the excess temperature inside the copper self-heating temperature-sensing device to the excess temperature on its surface is greater than 0.95, and the Biot number is less than 0.1.

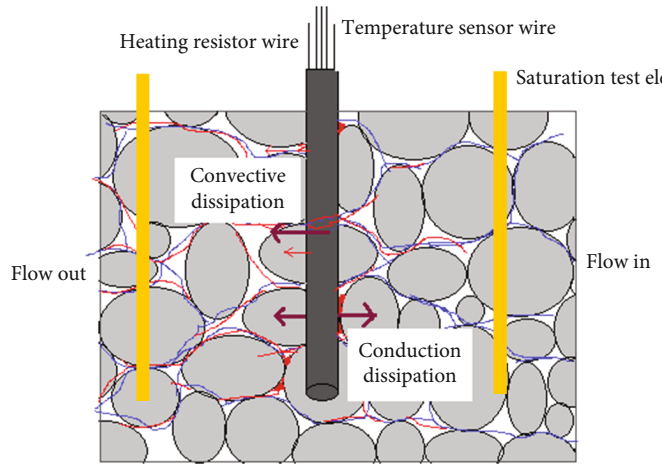

Figure 2: Schematic diagram of the monitoring model.

Therefore, its internal thermal resistance can be neglected, and the lumped parameter method can be used, which does not consider the heat conduction process inside the self-heating sensing device.

3. Self-Heating Temperature-Sensing Device

Based on the aforementioned assumptions, it is evident that if a temperature change is monitored at a certain measuring point in the model, it is necessary for the point to have a heating source and a temperature sensor capable of timely monitoring the temperature of the internal heat source. Self-heating temperature sensor devices with this function are commercially available, but their volume is large (φ4 mm × 3 cm), and they mostly use K-type thermocouples, which have a wide temperature range but low accuracy. In this study, PT100 temperature sensors are used instead of K-type thermocouples, miniature ceramic heating rods are used as internal heating sources, and φ4 mm × 1.5 cm copper tubes are used to encapsulate the temperature sensors and heating probes. To enhance thermal conductivity, the void inside the copper tube before encapsulation is filled with copper powder, and waterproof and insulating paint is used for sealing treatment. The self-heating temperature sensor probe (as shown in Figure 3) made based on the above process has a volume 50% smaller than that of similar products on the market, and its temperature measurement accuracy can reach ±0.1°C.

4. Analysis and Derivation of Heat Transfer Process

According to the quantitative relationship between the length, cross-sectional area, resistance, and heating time of a thermocouple heating conductor, when the heating resistor is located (situated) in air, there is no heat exchange between the heating resistor and the surrounding medium, and then

$$Q = P\tau' = cm(T_2 - T_1). \tag{3}$$

In the formula, P is the heating power of the heating conductor (W), t is the heating time (s), c is the equivalent specific heat capacity of the heating conductor (J/(kg·°C)), m is the mass of the heating conductor (kg), and T_2 and T_1 refer to the conductor temperature before and after heating, respectively.

Due to

$$\begin{aligned} \triangle T = T_2 - T_1 &= \frac{U^2}{10^{-6} c\rho_1\rho_2 l^2}\tau', \\ Q &= \frac{U^2}{\rho_1 l}\tau', \end{aligned} \tag{4}$$

where ρ_1 is the resistivity.

4.1. Analysis of Heat Conduction Status. During the cooling process of the self-heating temperature-sensing device, the heat loss mainly includes heat conduction (fluid and solid) and heat convection, which leads to the following relationship:

$$Q = Q_\lambda + Q_v, \tag{5}$$

where Q is the total calorific value of the model (J), Q_λ is the heat conduction between porous media and heating resistor (J), and Q_v is the thermal convection heat transfer between fluid and heating resistor (J).

When the heating resistor is located in the air, if there is no heat exchange between the heating resistor and the surrounding medium, there are

$$Q = Pt = cm(T_2 - T_1). \tag{6}$$

In the formula, P is the heating power of the heating conductor (W), t is the heating time (s), c is the equivalent specific heat capacity of the heating conductor (J/(kg·°C)), m is the mass of the heating conductor (kg), and T_2 and T_1 are the temperature of the conductor after heating and before heating (°C).

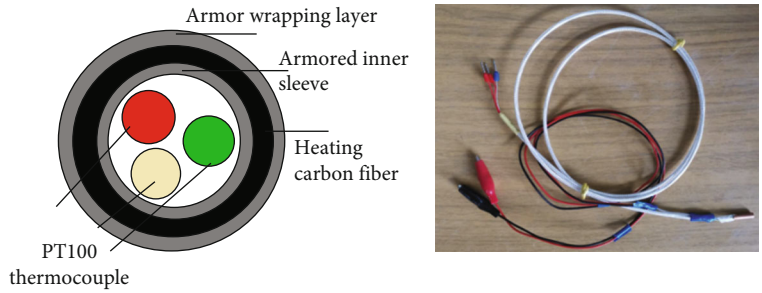

Figure 3: Self-heating temperature sensor component diagram: (a) component diagram; (b) finished product.

The heat conduction capacity of the self-heating temperature-sensing device in porous medium is

$$Q_\lambda = \frac{(1-\phi)S\lambda_{S_w}(T_2 - T_1)\tau}{\Delta x}, \tag{7}$$

where S is the surface area of measuring point device (m^2), ϕ is the porosity, λ_{S_w} is the thermal conductivity (W/(m·°C)), τ is the heat conduction time (s), and $\triangle x$ is the influence range of heat conduction (m).

4.2. Thermal Convection Analysis. Newton's law of cooling describes the process by which objects with a higher temperature than the surrounding environment transfer heat to the surrounding medium and gradually cool down when following the law. When there is a temperature difference between the object's surface and the surrounding environment, the amount of heat dissipated from a unit area per unit time is proportional to the temperature difference, and the proportionality coefficient is called the convective transfer coefficient. Newton's law of cooling was determined experimentally by Newton in 1701, and it is well matched with actual conditions in forced convection. In natural convection, it only holds when the temperature difference is not excessively large. It is one of the basic laws of heat transfer and is used to calculate the amount of convective heat.

The heat exchange between the heating resistor and the percolating fluid is calculated using Newton's law of cooling:

$$Q_v = \phi Sh(T_s - T_o)\tau, \tag{8}$$

where Q_v is the convective heat transfer between fluid and heating resistor; S is the surface area of measuring point device; T_s is the heating resistor surface temperature, which can be directly read through temperature sensors; T_o is the temperature of seepage fluid, which can be approximately equal to the experimental ambient temperature; and h is the convective heat transfer coefficient.

ϕ, S, T_s, and T_f are known, and only the convective heat transfer coefficient h is unknown, so the study of convective heat transfer conditions is transformed into a study of the convective heat transfer coefficient [19, 20]. Through analysis, it is known that the heat transfer coefficient is related to the percolation velocity, heating resistance properties, specific heat, density, kinematic viscosity coefficient, and thermal conductivity of the mixed percolation fluid.

$$h = f(u, l, \rho_w(f_w), c_w(f_w), \nu_w(f_w), \lambda_w(f_w)). \tag{9}$$

In the equation, fluid density of mixed seepage flow is

$$\rho_l(f_w) = \rho_w \times f_w + \rho_o \times (1 - f_w). \tag{10}$$

Specific heat of mixed seepage fluid is

$$c_l(f_w) = c_w \times f_w + c_o \times (1 - f_w). \tag{11}$$

Kinematic viscosity is

$$\nu_l(f_w) = \nu_w \times f_w + \nu_o \times (1 - f_w). \tag{12}$$

Thermal conductivity (Lu thermal conductivity model) is

$$\lambda_l(f_w) = \lambda_w \times f_w + \lambda_o \times (1 - f_w). \tag{13}$$

The above parameters can be determined through testing or table:

$$\begin{aligned} f_w &= \frac{1}{1 + (1/\mu_r)(k_{ro}/k_{rw})}, \\ \frac{K_{ro}}{K_{rw}} &= e^{-aS_w}\left(b + ce^{aS_w}\right)^2. \end{aligned} \tag{14}$$

Then,

$$f_w(S_w) = \frac{1}{1 + (1/\mu_r)e^{-aS_w}\left(b + ce^{aS_w}\right)^2}. \tag{15}$$

At this time, the formula for the heat transfer coefficient can be simplified to

$$h = f(u, S_w). \tag{16}$$

It is a function of seepage velocity and water content.

4.3. Derivation of Theoretical Equation for Seepage Monitoring. The heating resistor is placed vertically inside the reservoir model, and the heat exchange during the percolation process occurs in the form of single-tube heat transfer outside the fluid [21–24].

Based on the principle of similarity of characteristic numbers and the characteristic correlation formula, the velocity expression can be derived. The definitions and calculation processes of each characteristic number are as follows:

(a) Reynolds number Re: a measure of the ratio of inertial force to viscous force, which is a quantitative indicator of the flow state, defined as

$$\mathrm{Re} = \frac{u\rho\sqrt{k}}{17.5\mu\phi^{3/2}}, \tag{17}$$

where μ is the viscosity (mPa·s), ρ is the density (g/mL), k is the permeability (mD), and ϕ is the porosity

(b) Prandtl number Pr: the ratio of the momentum diffusion thickness to the heat diffusion thickness, which represents the relative size of the momentum diffusion ability and the heat diffusion ability of the fluid and is defined as

$$\mathrm{Pr} = \frac{\nu}{\lambda_l}. \tag{18}$$

(c) Nusselt number Nu: the dimensionless temperature gradient of a fluid near a wall, defined as

$$\mathrm{Nu} = \frac{hd}{\lambda_l}. \tag{19}$$

According to the heat transfer characteristics of the fluid sweeping through a single tube, the relationship between the characteristic numbers can be determined as follows:

$$\mathrm{Nu} = C\,\mathrm{Re}^n\mathrm{Pr}^{1/3} \tag{20}$$

The values of C and n are related to Reynolds number. Bring each feature number into the correlation equation:

$$\frac{hd}{\lambda_l} = C\left(\frac{u\rho\sqrt{k}}{17.5\mu\phi^{3/2}}\right)^n\left(\frac{\nu}{\lambda_l}\right)^{1/3}. \tag{21}$$

After sorting, it can be concluded that

$$h = C\frac{\lambda_l}{d}\left(\frac{\rho\sqrt{k}}{17.5\mu\phi^{3/2}}\right)^n\left(\frac{\nu}{\lambda_l}\right)^{1/3}u^n. \tag{22}$$

Let:

$$D = C\frac{\lambda_l}{d}\left(\frac{\rho\sqrt{k}}{17.5\mu\phi^{3/2}}\right)^n\left(\frac{\nu}{\lambda_l}\right)^{1/3}. \tag{23}$$

The relationship between heat transfer coefficient and flow rate can be obtained as follows:

$$h = Du^n. \tag{24}$$

Bringing equations (6)–(8) into (5),

$$cm = \phi Sh\tau + \frac{(1-\phi)S\lambda_s\tau}{\Delta x}. \tag{25}$$

Bringing (23) and (24) into (25),

$$cm = \phi SC\frac{\lambda_l}{d}\left(\frac{\rho\sqrt{k}}{17.5\mu\phi^{3/2}}\right)^n\left(\frac{\nu}{\lambda_l}\right)^{1/3}u^n\tau + \frac{(1-\phi)S\lambda_s\tau}{\Delta x}. \tag{26}$$

After organizing the above equation, the total flow velocity of the fluid can be obtained as follows:

$$u = \frac{17.5\mu\phi^{3/2}}{\rho\sqrt{k}}\sqrt[n]{\left(\frac{\lambda_l}{\nu}\right)^{1/3}\frac{d}{\lambda_l\phi C}\left(\frac{cm}{\tau} - \frac{(1-\phi)\lambda_s}{\Delta x}\right)}. \tag{27}$$

Based on the distribution of saturation in the reservoir, the corresponding water cut can be calculated using the partial flow equation. Multiplying the total flow rate by the water cut yields the expression for the water phase flow rate, which can be multiplied by the oil cut to obtain the oil phase flow rate:

$$\begin{aligned} \mathrm{v}_w &= u \times f_w(S_w), \\ \mathrm{v}_o &= u \times (1 - f_w(S_w)). \end{aligned} \tag{28}$$

5. Heat Transfer Coefficient and Saturation Plate in Reservoir Model Testing and Seepage Monitoring Test

5.1. Heat Transfer Coefficient of Reservoir Model. When multiphase fluids exist in the reservoir model, their thermal conductivity is affected by multiple factors. In order to provide basic parameter support for monitoring and calculating flow velocity in the reservoir model, it is necessary to test the thermal conductivity under different saturation conditions. The testing principle is as follows [21]:

$$\lambda = \frac{q'}{4\pi}\frac{\ln\left[(t_2/t_1)(t_1 - t_h)/(t_2 - t_h)\right]}{\left[T(t_2) - T(t_1)\right]}, \tag{29}$$

where q' is the heating power per unit length (W/m); t_1, t_2, and t_h refer to the test recording time (s); and $T(t_1)$ and $T(t_2)$ record the corresponding temperature test value at the time of testing (°C).

Firstly, the principle of steady-state method for measuring phase permeability is adopted. A core sample with a specific saturation condition is produced by injecting oil and water into a saturated oil-water core at a certain ratio. The

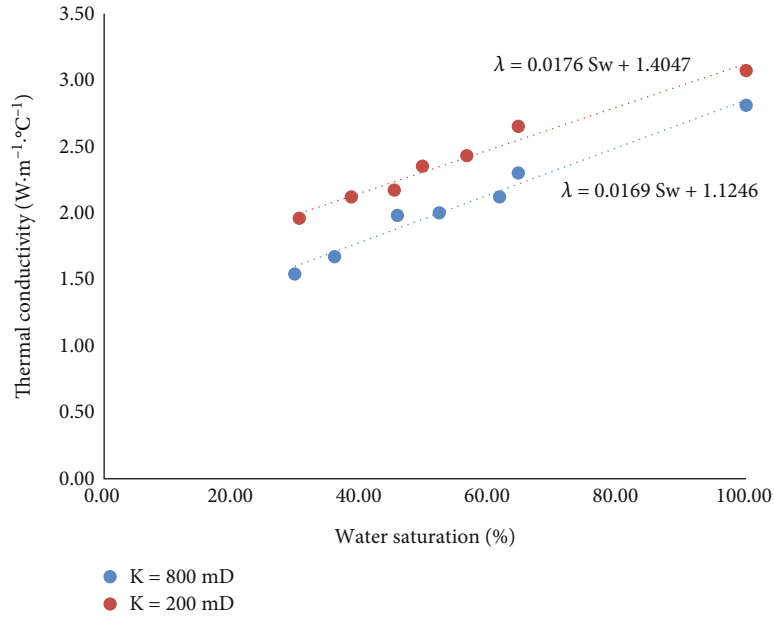

Figure 4: Relation curve between thermal conductivity and water saturation of rock.

thermal conductivity of the core sample is then measured using a thermal conductivity meter.

From Figure 4, it can be seen that the water saturation and thermal conductivity of the rock core exhibit a linear relationship:

$$\lambda(S_w) = aS_w + b. \tag{30}$$

5.2. Saturation Test of Porous Medium. The distribution of oil saturation in the reservoir model is the material basis for oil displacement experiments and analysis. Various saturation testing methods in small core models include extraction, CT scanning, and nuclear magnetic resonance, which can achieve good testing results. However, monitoring of saturation in large-scale physical simulations is limited by the size of the model to be tested and the capabilities of the corresponding testing equipment, requiring other indirect methods for testing. Currently, the testing method for oil saturation in large-scale physical simulations is based on the Archie formula in well logging theory (as shown in Figure 5). First, two symmetrical and equidistant (1.5 cm in this study) test electrodes (insulating enameled nickel-cobalt alloy wire: $\varphi 0.5\,\text{mm} \times 2\,\text{cm}$) are embedded in the model. Then, a controlled alternating current is intermittently applied between the two electrodes, and the resistance between the two electrodes is monitored. Combining the prepared water saturation and resistivity chart, the resistance value is converted into oil saturation using a computer.

Crude oil exhibits a very high resistivity and can even be regarded as nonconductive, so when there is oil-water two-phase flow in the reservoir model, the measured resistivity is mostly the water phase resistivity. Due to the difference in resistivity in the oil-water two-phase flow, which can reach 5-8 orders of magnitude, the measured resistivity change is the change in water saturation in the reservoir model. The resistivity in the reservoir model is affected by several factors, such as porosity, connectivity, salinity of formation water, and test temperature, which have a great influence on the test results. Since the conductivity and dielectric constant of the reservoir model are both functions of frequency, when the frequency of the external voltage field changes, the electrodes will be affected by the frequency dispersion effect of various electrical parameters of the rock, which will make the testing process unstable. When the test frequency is controlled at 10^5 Hz, the frequency dispersion phenomenon has a small impact on the results, so this study chooses a frequency of 10^5 Hz.

After measuring the formation resistivity, the water saturation can be calculated using the Archie formula:

$$I = \frac{R_t}{R_0} = S_w{}^{-n}. \tag{31}$$

In the formula, R_t is the resistivity of the rock sample containing a certain oil and water saturation (Ω), R_0 is the rock resistivity of 100% saturated water (Ω), S_w is the water saturation (%), and n is the saturation index.

The methods for determining R_t and n include core displacement experiment (columnar core displacement experiment) and empirical coefficient method.

Due to the small size of the probe, the size of the electrode ring and the size of the electrode system are on the same order of magnitude, so the requirement for a point source cannot be met and the electrode system coefficients cannot be determined analytically. The influence of some uncertain factors on the electrode during the compression process can greatly affect the outcomes of numerical simulation. Therefore, only a series of uniform media with known conductivity can be used to calibrate the electrode, and the

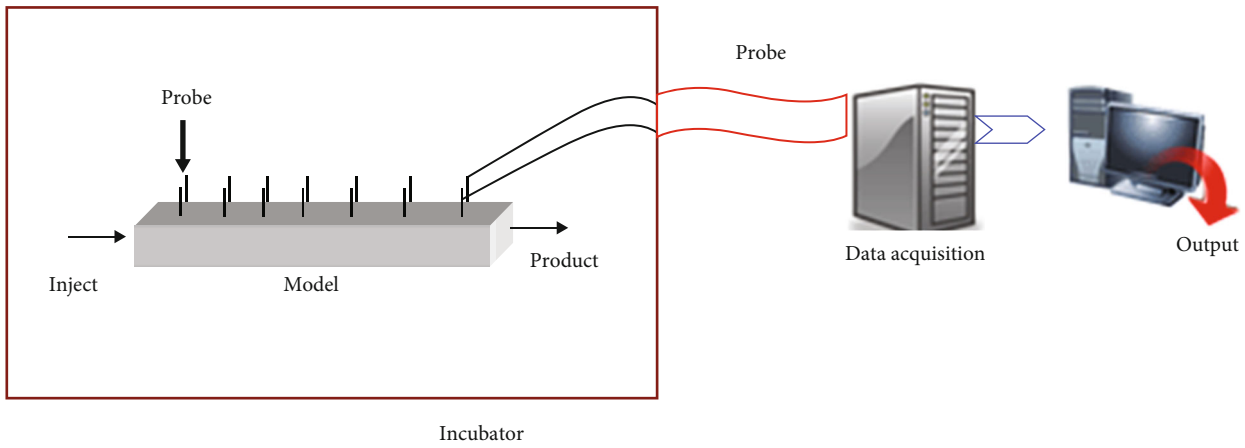

Figure 5: Movable fluid saturation monitoring system.

relationship between the measured value of the probe resistance and the solution resistivity can be established through regression.

The methods for determining n and b include core displacement experiments (columnar core displacement experiments) and empirical coefficient methods. Through the results of resistivity tests at different water saturation levels, a relationship diagram between water saturation and resistivity can be obtained (as shown in Figure 6).

Given the minor variation in saturation in the later stage of ultrahigh water cut, the measured resistivity also tends to be low. In order to better reflect the saturation distribution characteristics at this stage, it is essential to correct the measurement results in combination with the model output oil production.

5.3. Seepage Monitoring Test. A 50 cm long sand-filled tube model (as shown in Figure 7) was made using a 2.5 cm inner diameter plexiglass tube. The effective permeability of the sand-filled tube model was controlled by filling it with quartz sand of a certain mesh ratio and applying a certain degree of filling pressure. Arrange self-heating temperature probes and saturation electrodes at 1/3 of the sandpack tube, and arrange the same test points at 2/3 of the sandpack tube as backup and verification test points for repeatability.

The purpose of this saturation monitoring is to verify the possibility and reality of accurately obtaining oil-water saturation using the electrode method. The model is injected at one end with simulated oil and water simultaneously using two pumps at a certain ratio (oil-to-water ratio: 1, 0.8, 0.6, 0.4, 0.2, 0). The viscosity of the oil is 10 μm^{-2} (25°C), and the salinity of water is 8000 ppm. The total liquid injection rate of oil-water two-phase flow is 0.5 mL/min, 1 mL/min, and 1.5 mL/min. Through the above theory and device, the average flow velocity of oil and water phases under different water cut conditions can be measured. The test and calculation results are compared with the actual injection velocity, as shown in Figures 8 and 9.

By comparing the flow velocities of the water and oil phases under different injection conditions, it is evident that the method proposed in this paper for detecting the flow

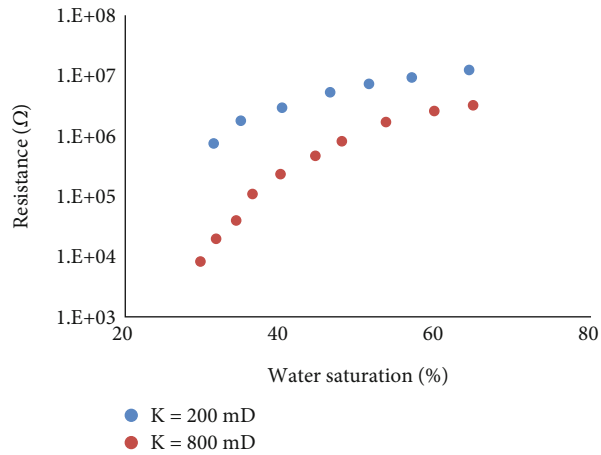

Figure 6: Chart of the relationship between water saturation and resistivity.

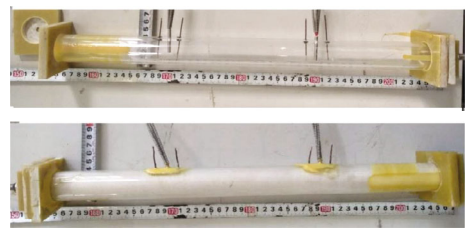

Figure 7: Verification model of flow rate test method.

velocity in porous media exhibits robust applicability and can accurately provide relatively accurate velocity test results under different saturation conditions. Compared to the higher injection rate of 1.5 mL/min, the detection value of the flow velocity of the oil-water two-phase flow at the injection rate of 0.5 mL/min is in better agreement with the true flow velocity. The possible reason is that when the injection rate is high, the oil-water two-phase flow in the porous medium no longer conforms to the Darcy flow law, resulting in a certain degree of deviation in the test results.

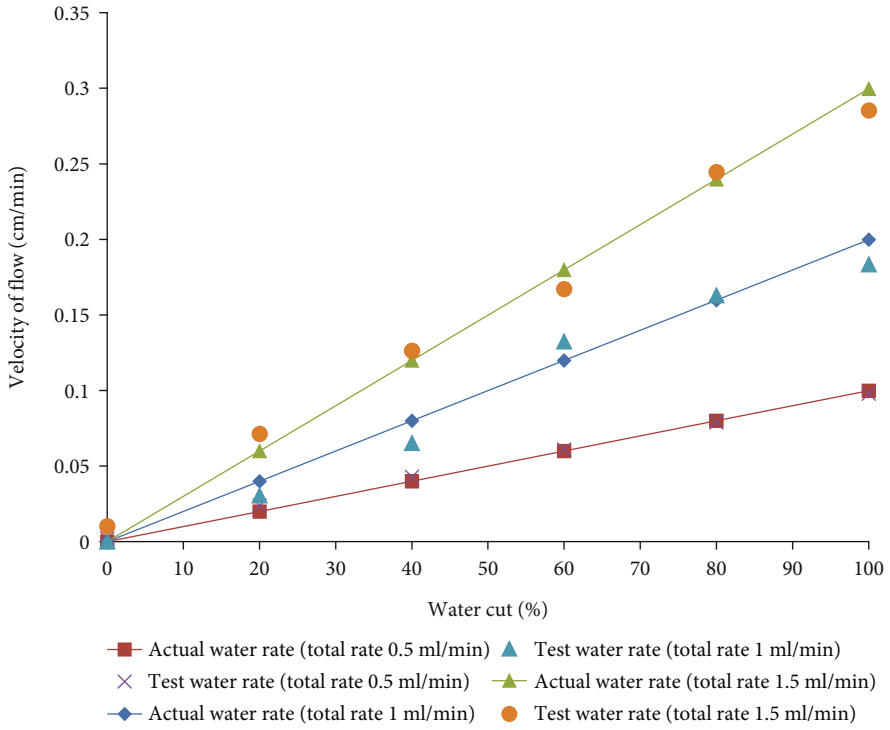

Figure 8: Comparison of actual and test flow velocities of water phases.

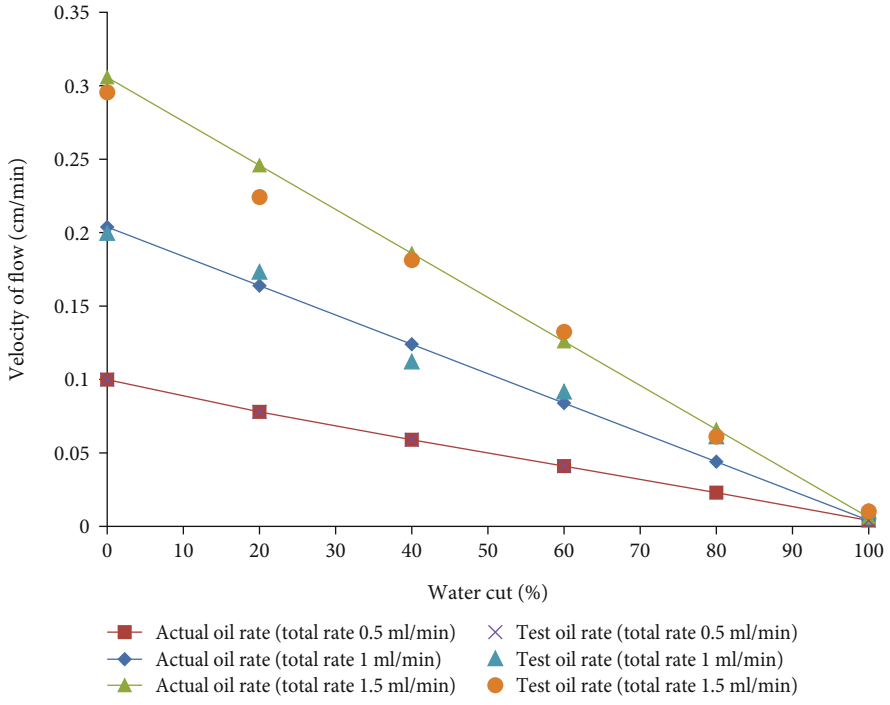

Figure 9: Comparison of actual and test flow velocities of oil phases.

6. Conclusion

(1) Based on the analysis of internal heat transfer in porous medium, the theoretical equation of seepage monitoring is established, which provides a strong theoretical support for the establishment and application of self-heating multiphase seepage detection method. Due to certain simplifications and assumptions made during the equation derivation process, the theory still needs further testing and improvement

(2) By measuring the resistivity of porous medium under various water cut states, to establish the corresponding chart, the water saturation and water cut of porous medium at different times can be determined

(3) By comparing the actual two-phase seepage velocity and velocity test results in porous medium under varying heating power, it can be seen that the accuracy can reach over 95%, which verifies the accuracy and reliability of the proposed method in this paper

Data Availability

The data used to support the findings of this study are included within the article.

Conflicts of Interest

The authors declare that they have no conflicts of interest.

Acknowledgments

This study was supported by the Key Technologies for Greatly Improving Oil Recovery in Offshore Oil Fields (No. KJGG2021-05), a technology project of China National Offshore Oil Co., Ltd.

References

[1] Z. Wu and S. Hanzhou, "Study on seepage heat monitoring of earth-rockfill dams based on flow-heat coupled model," *Rock and Soil Mechanics*, vol. 36, no. 2, pp. 584–590, 2015.

[2] Q. Chuanyong and H. Lu, "Experimental study on the use of heated optical fibers in channel leakage monitoring," *Water Conservancy Technical Supervision*, vol. 25, no. 2, pp. 48–51, 2017.

[3] G. Xiaoqing, X. Qing, and N. Jing, "Progress in the theoretical study of seepage and thermal monitoring of earth-rock dams," *Journal of Yangtze River Institute of Science and Technology*, vol. 31, no. 7, pp. 119–124, 2014.

[4] J. Xiaoyi, "Innovation and application of parallel electrical detection and directional processing technology for reservoir leakage," *China Water Resources*, vol. 18, pp. 68-69, 2015.

[5] T. Wang, "Application of electrical probing in detecting dam leakage in Tianhuding reservoir," *Water Conservancy Science and Technology*, vol. 4, pp. 70–72, 2016.

[6] X. Lin, "Application of high-density electrical method in the seepage investigation of Dengyun reservoir dam," *Water Conservancy Construction and Management*, vol. 39, no. 8, pp. 68–71, 2019.

[7] F. Chungang, G. Huaiguang, Y. Lu, K. Zhiquan, and J. Yongmei, "Transient electromagnetic method for detecting hidden dangers and leakage of embankments," *Dam Observation and Geotechnical Testing*, vol. 4, pp. 30–32, 2001.

[8] F. Chungang, J. Yongmei, G. Huaiguang, and Y. Lu, "Detection of hidden dangers in embankments using frequency-domain electromagnetic method," *Water Resources and Hydropower Technology*, vol. 2, pp. 54–57, 2002.

[9] C. Xinghai, Z. Pingsong, J. Xiaoyi, and T. Lei, "Geophysical detection technology and progress of reservoir dam leakage," *Journal of Engineering Geophysics*, vol. 11, no. 2, pp. 160–165, 2014.

[10] S. Cong and H. Liguo, "Forward simulation study on the quality detection of reinforced concrete underground diaphragm wall using elastic wave method," *Science Technology and Engineering*, vol. 14, no. 9, pp. 93–98, 2014.

[11] W. Ligang, "Application of fluorescent tracer method in dam leakage exploration," *Water Resources Planning and Design*, vol. 10, pp. 184–186, 2018.

[12] X. Henglin, Z. Jinfeng, and J. He, "Research on flow velocity measurement method based on distributed optical fiber sensing technology," *Rock and Soil Mechanics*, vol. 30, no. 11, pp. 3543–3547, 2009.

[13] X. Henglin, H. Bao, C. Wang, and C. Desuo, "Research on seepage monitoring theory based on distributed optical fiber sensing technology," *Rock and Soil Mechanics*, vol. 10, pp. 2794–2798, 2008.

[14] X. Xu, *Research on Leakage Monitoring Method Based on Distributed Optical Fiber Temperature Sensor Technology*, Hubei University of Technology, 2012.

[15] Q. Li, Y. Han, X. Liu, U. Ansari, Y. Cheng, and C. Yan, "Hydrate as a by-product in CO_2 leakage during the long-term sub-seabed sequestration and its role in preventing further leakage," *Environmental Science and Pollution Research*, vol. 29, no. 51, pp. 77737–77754, 2022.

[16] Q. Li, F. Wang, Y. Wang et al., "Experimental investigation on the high-pressure sand suspension and adsorption capacity of guar gum fracturing fluid in low-permeability shale reservoirs: factor analysis and mechanism disclosure," *Environmental Science and Pollution Research*, vol. 29, no. 35, pp. 53050–53062, 2022.

[17] F. Yin, Y. Gao, Y. Chen, B. Sun, S. Li, and D. Zhao, "Numerical investigation on the long-term production behavior of horizontal well at the gas hydrate production site in South China Sea," *Applied Energy*, vol. 311, article 118603, 2022.

[18] Z. Wu and S. Hanzhou, "Coupled analysis of temperature field and variable physical property seepage field at dam site," *Journal of Water Resources*, vol. 41, no. 6, pp. 703–710, 2010.

[19] G. Janardhana Reddy, B. Kethireddy, M. Kumar, and O. Anwar Bég, "Transient analysis of thermal convection of Casson fluid in a vertical cylinder in porous media: visualization of entropy generation and heat transfer," *Journal of Central South University*, vol. 26, no. 5, pp. 1342–1361, 2019.

[20] Y. Mao, Y. Hunian, and X. Xu, "Experimental study on fluid thermal convection in porous media," *Journal of Huazhong University of Science and Technology*, vol. 5, pp. 95–98, 1989.

[21] R. Lin, L. Xiaochen, J. Liang, and L. Da, "Experimental study on the heat transfer characteristics of mixed convection in a circular tube with low-temperature seawater external sweep," *Journal of China University of Petroleum (Natural Science Edition)*, vol. 42, no. 6, pp. 133–138, 2018.

[22] Z. Xiuxia, R. Lin, L. Xiaochen, and D. Yang, "Construction and application of a low-temperature seawater external sweeping circular tube convection heat transfer experimental platform," *Experimental Technology and Management*, vol. 36, no. 3, pp. 233–237, 2019.

[23] K. Xiyang, X. Zhu, and Q. Liao, "Lattice Boltzmann method simulation of flow and heat transfer in a swept circular tube," *Chemical Engineering*, vol. 38, no. 4, pp. 21–24, 2010.

[24] L. Jishan, "Testing of thermophysical properties of reservoir rocks," *Journal of Daqing Petroleum Institute*, vol. 33, no. 5, pp. 23–26, 2009.